Comparison of helium glow and lithium evaporation wall conditioning techniques in achieving high performance H-mode discharges in NSTX

R. Maingi[1], J.M. Canik[2], R.E. Bell[1], D.P. Boyle[3], A. Diallo[1], R. Kaita[1], S.M. Kaye[1], B.P. LeBlanc[1], S.A. Sabbagh[4], F. Scotti[5], V.A. Soukhanovskii[5], and the NSTX-U team

Email: rmaingi@pppl.gov

[1] *Princeton Plasma Physics Laboratory, 100 Stellarator Road, Princeton, NJ 08543 USA*

[2] *Oak Ridge National Laboratory, Oak Ridge, TN, USA*

[3] *Princeton University, Princeton, NJ, USA*

[4] *Columbia University, New York, NY, USA*

[5] *Lawrence Livermore National Laboratory, Livermore, CA USA*

1. Introduction

Good discharge reproducibility and H-mode performance was realized in the National Spherical Torus Experiment (NSTX) with an extensive wall-conditioning program. The graphite plasma-facing components were baked for several weeks to 350 ºC at the beginning of a campaign, with extensive deuterium and helium glow discharge cleaning (HeGDC). Periodic boronization was used to reduce oxygen content[1, 2], and enabled reliable H-mode access[3]. Daily run preparation included 15-30 minutes of pre-run HeGDC, followed by inter-discharge HeGDC of 9-14 minutes, depending on the target discharges, with a resulting inter-discharge time of 15-20 minutes[2]. With the development of inter-discharge lithium evaporation[4], however, the need for both inter-discharge HeGDC and lithium evaporation became questionable.

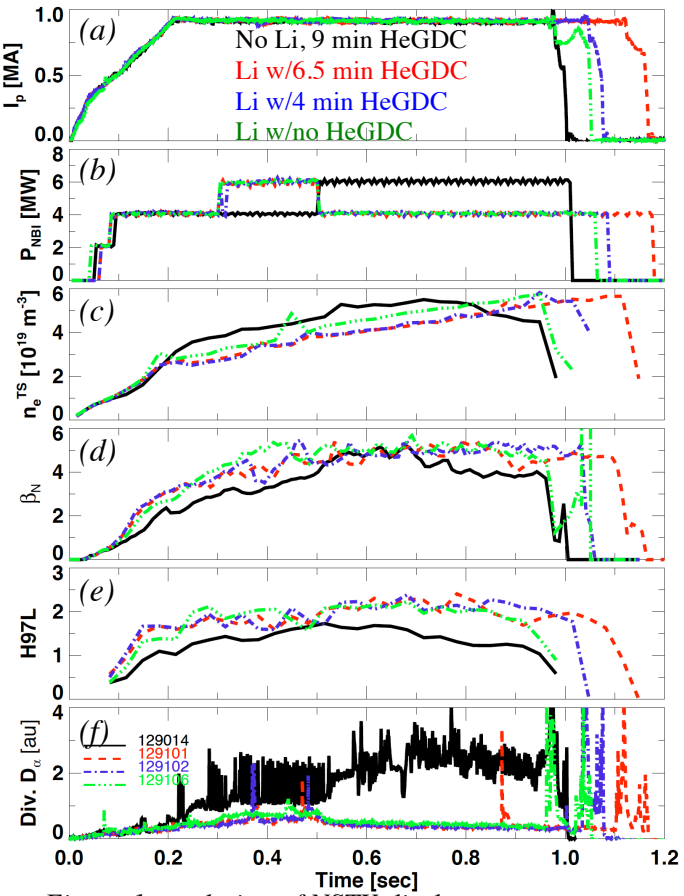

Figure 1: evolution of NSTX discharge parameters with variable HeGDC time preceding Li evaporation. A reference ELMy discharge without lithium and with standard HeGDC is also shown.

Following the NSTX wall-conditioning studies with boronized plasmas and inter-discharge HeGDC, lithium injection was utilized, first via pellets[5], and then via evaporation[6], building on the positive experience with lithium in TFTR[7]. The evaporative coatings in NSTX showed an increase in energy confinement[8, 9], with observed elimination of Type I ELMs[10]. The ELM elimination was correlated with reduced wall fueling, and also an inward shift of the pedestal density and pressure profiles[11, 12]. While the first of these lithium evaporation experiments used HeGDC prior to lithium usage, the wall fueling reduction from lithium

evaporation[13] raised the possibility of complete elimination of HeGDC. This would simplify operational procedures, while reducing the inter-discharge cycle time. To evaluate this, a sequence of discharges was conducted with the HeGDC time before lithium evaporation reduced sequentially from 10 minutes down to zero. The lithium dose following HeGDC, the neutral beam heating, and gas fueling were held constant, as described below.

2. Elimination of Helium Glow Discharge Cleaning during Lithiumization

To assess the viability of operation without HeGDC and directly compare with inter-discharge lithium evaporation, experiments were conducted in which lithium evaporation was used while systematically reducing the inter-discharge HeGDC from the standard 9-10 minutes to zero[14]. Good discharge reproducibility without HeGDC was achieved with lithium evaporation doses of 100 mg or higher; evaporations of 200-300 mg typically resulted in very low ELM frequency or ELM-free operation, reduced recycling, and improved energy confinement.

Figure 1 compares four discharges: a reference 9 min HeGDC and no Li (black - #129014), 6.5 min HeGDC followed by Li evaporation (red - #129101), 4 min HeGDC followed by Li (blue - #129102), and no HeGDC followed by Li evaporation (green). The lithium dose was ~ 500mg in each of these discharges. The reference discharge was taken before any Li had been used in this campaign. Note that the discharge pulse length was modestly reduced with decreasing with HeGDC duration. Figure 1b shows that the neutral-beam power waveforms were slightly different: the reference discharge ramped from 4 to 6 MW, while the discharges with lithium were ramped down for 6 to 4 MW. For this reason, time comparisons in this paper will be made during the 4 MW phase.

Figure 1c shows that the line-averaged density from Thomson Scattering exhibited different ramp rates. The biggest change in dN/dt occurred with deployment of Li (red vs. other curves). The impact of reducing the HeGDC is more subtle: reducing the HeGDC time from 9 min to 0 has a modest impact in dN/dt. Figure 1d shoes that the peak normalized pressure, β_N, was comparable between these discharges. Figure 1e shows that the discharges with lithium treatment had substantially energy confinement normalized to the ITER-97 L-mode scaling law[15]. Finally Figure 1f shows that the divertor D_α emission was reduced with lithium coating, although it was marginally higher when HeGDC was eliminated. Note that while the reference discharge was ELMy, the lithium evaporation rate was sufficient to insure

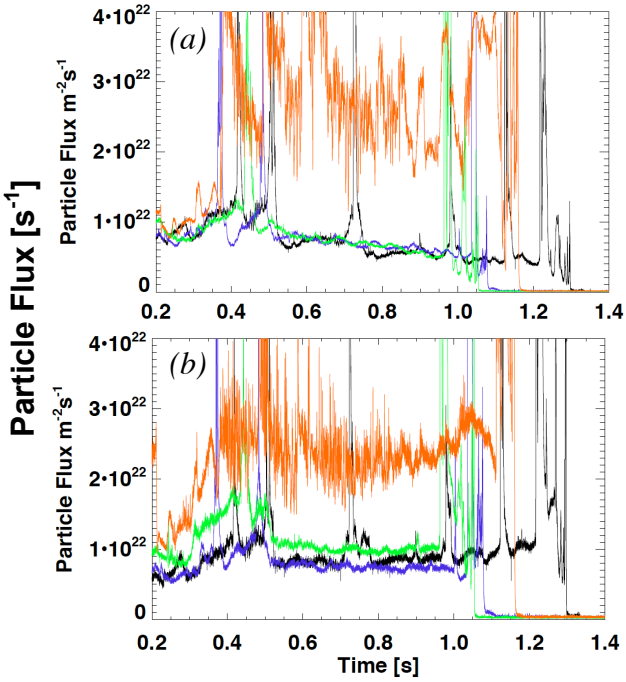

Figure 2: Equivalent particle flux by integrating D_α emission in (a) near SOL, and (b) far SOL, from discharges with 10 min HeGDC (black), 6.5 min HeGDC (red), and no HeGDC (green). Also shown is a discharge with 10 min HeGDC but no Li dose (orange). Additional information is in the text.

ELM-free H-mode operation (Figure 1f).

The radial profile of the divertor D_α emission was compared for the discharges of the HeGDC scan[14]. This comparison showed that the D_α emission near the outer strike point was unaffected by the duration of HeGDC, but also that the D_α emission in the far SOL increased with decreasing HeGDC time. To quantify the impact of the radial variations on the total flux, the photon flux was converted to equivalent local ion flux by $\Gamma = \gamma \int_{R1}^{R2} D_\alpha(r) 2\pi R(r) dr$, where γ is the number of ionizatons per photon (assumed to be 20 for an ionizing plasma), for several discharges from the previous figures. Figure 2 compares the time evolution of the fluxes for the near SOL profiles (i.e. R1 = 0.35m, R2=0.45m, panel (a)) and the far SOL fluxes (i.e. R1 = 0.45m, R2=0.55m, panel (b)). For reference the outer strike point was ~ 0.35m. Figure 2a shows that the near SOL particle flux for the three discharges with lithium evaporation are comparable, and all are much lower than for the discharge with no lithium evaporation. As can be seen in Figure 2b, the far SOL particle flux is higher for the discharge without HeGDC (#129106 green) than the ones with 6.5 min HeGDC (129102 blue) and 10 min HeGDC (129100 black). For context, the flux from a reference discharge with no lithium evaporation and 10 min HeGDC (#129096 orange) is also plotted[14]. One speculation for the similarity in the near SOL flux is that the intense plasma-bombardment near the outer strike point tends to saturate and regulate the surface rapidly, i.e. largely independent of the preceding HeGDC. One tentative mechanism for this is that the high PFC temperature near the strike point may hasten the diffusion rate from the bulk back to the surface. However the lower flux in the far SOL for discharges with HeGDC means that the equilibrium surface particle flux can be affected in low fluence zones, i.e. that the HeGDC can reduce D_α in those regions. It is interesting to note that the flux reduction does not depend on the duration of HeGDC, i.e. deployment of small durations is sufficient for flux control[14].

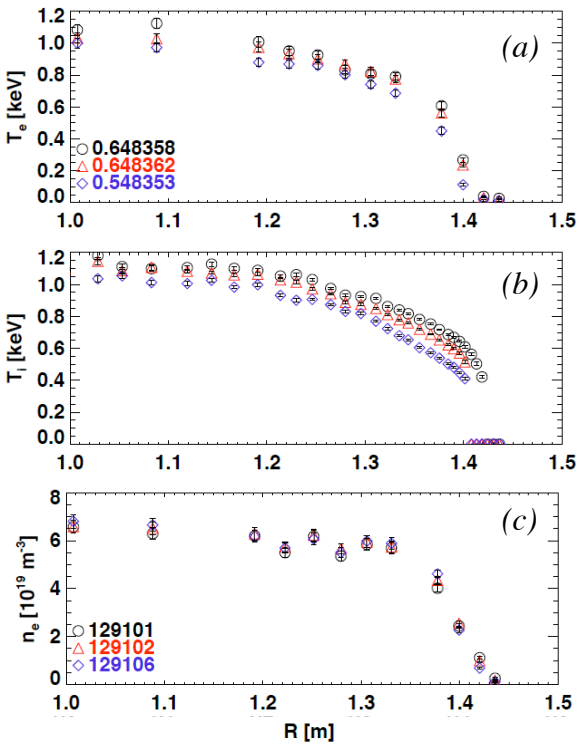

Figure 3: comparison of T_e, T_i and n_e profiles for discharges with 6.5 min HeGDC (black diamonds), 4 min HeGDC (red triangles), and no HeGDC (blue circles). All discharges were followed by ~500mg of lithium evaporation.

One final aspect deserving comment is the effect of the HeGDC duration on the edge plasma profiles. A comparison of the temperature profiles at fixed density profile for an individual time slice from three discharges is shown in Figure 3. Here there appears to be a consistent increase of both T_e and T_i with increasing HeGDC time; comparing no HeGDC to 6.5 min HeGDC shows up to a 30% increase. From these experiments, we conclude that far SOL recycling control can be provided with minimal HeGDC, as low as 4 min. On the other hand, the edge temperatures may continue to

increase with increasing HeGDC duration, i.e. there may be additional benefit from using HeGDC of more than 4 min duration.

The inverse experiment, i.e. when lithium evaporation was terminated, and inter-discharge HeGDC was re-initiated, was also conducted, although in a less controlled manner than the scan just reported. Here a systematic increase in HeGDC duration was used for discharge reproducibility, which was nonetheless accompanied by a decrease in external fueling required for constant density. Generally the trends reported above were also observed here, albeit in a reverse time sequence.

Finally, an experiment in which a large lithium dose (~200g, ~1000 times the typical inter-discharge evaporation) prior to operations was conducted. In this case, about 100 plasma discharges over three run days were conducted with neither inter-discharge Li evaporation nor HeGDC. Nearly all of these achieved H-mode, but the pulse lengths and performance

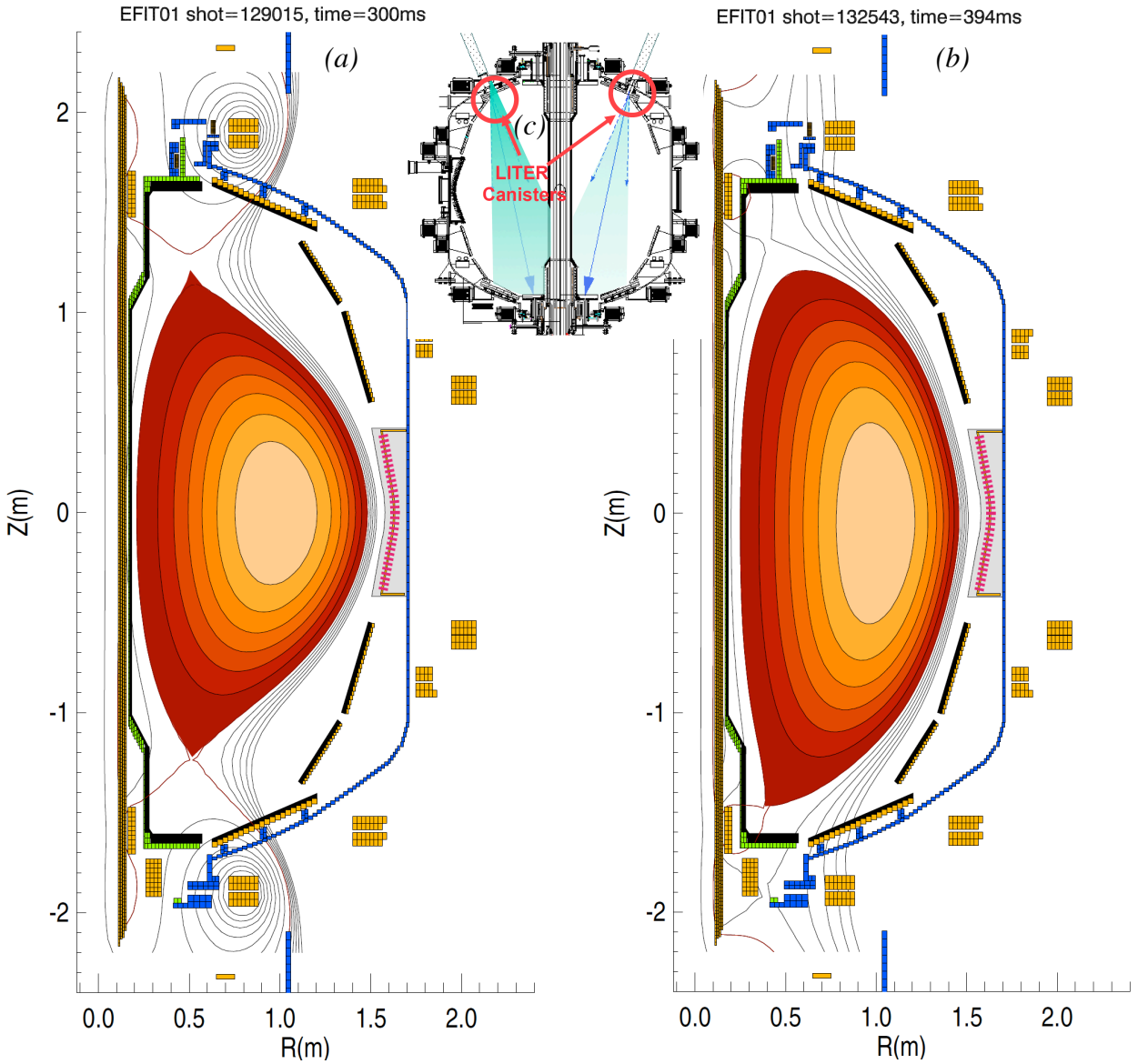

Figure 4: comparison of (a) moderate and (b) highly-shaped plasmas with centroid of lithium evaporator deposition in inset (c).

were irreproducible. At the end of the sequence, recycling started to slowly increase. Hence external fueling was decreased, and inter-discharge HeGDC was resumed, without additional lithium evaporation.

3. Comparison of lithiumization in highly shaped and moderately shaped plasmas

NSTX-U is designed to operate with highly shaped plasmas (i.e. high elongation $\kappa \sim 2.3$ and triangularity $\delta \sim 0.8$)[16, 17]. Thus the interplay between shape and efficacy of lithium conditioning was studied, by comparing previous analysis of moderately shaped discharges[11, 13, 18-20] with strongly shaped ones, as a function of lithium dose.

The NSTX experiments and analysis mentioned above were performed in a moderate $\delta \sim 0.45$, $\kappa \sim 1.8$ boundary shape; we now present analysis of a similar experiment with $\delta \sim 0.65$, $\kappa \sim 2.2$. Similar global trends between these two experiments regarding discharge modifications as a function of lithium evaporation were observed[21]. A comparison of these boundary plasma shapes is shown in Figure 4, along with a schematic of two toroidally separated overhead LIThium EvapoRators ("LITER") in NSTX. Note in particular that the centroid of LITER deposition was very close to the outer divertor strike point in the highly shaped plasma, whereas it was in the private flux region in the weakly shaped plasma.

This was the first experiment in this particular campaign in which lithium was used; previous discharges used periodic boronization and inter-shot HeGDC. After obtaining ~ 10 reference discharges with both 5 and 6 MW neutral-beam injected (NBI) power, lithium was introduced for seven discharges at a dose ~ 150 mg. The next eight discharges used ~ 250 mg per discharge. The next six discharges varied the lithium dose between 250 and 500 mg each, with some alternation of high and low doses to assess hysteresis. The following eight discharges used ~ 450 mg per discharge, while the final nine discharges used ~ 500-550 mg per discharge. The effects observed in this experiment depended mostly on the lithium dose between discharges, with a minor effect related to the integral dose[21, 22].

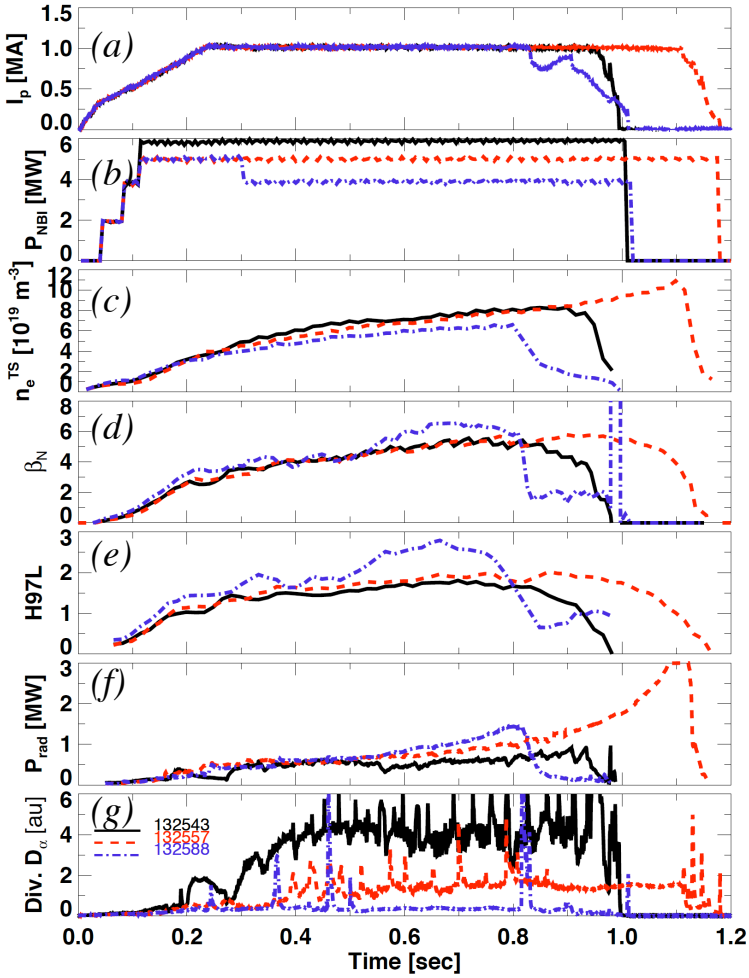

Figure 5: comparison of reference discharge (black) with intermediate (red) and high (blue) pre-discharge lithium evaporation. The NBI power was reduced modestly to stay below the global stability limit.

A comparison of the evolution of

three discharges during the experiment[22] is presented in Figure 5. These three discharges, plus a fourth one, were used in the interpretive SOLPS modeling to quantify the reduction in divertor recycling coefficient and edge cross-field transport. Panel (a) displays plasma current I_p, panel (b) the NBI power P_{NBI}, panel (c) the line-averaged electron density, panel (d) the normalized pressure β_N, panel (e) the energy confinement time normalized to the ITER H97 L-mode scaling law[15], panel (f) the radiated power in the core, and panel (g) the lower divertor D_a emission. The P_{NBI} was reduced from 6 -> 5 -> 4 MW with increasing lithium dose to keep the plasma below the global stability limit $\beta_N \leq 6$ (panels (b), (e)). The normalized confinement improved with increassing lithium dose (panel (e)). Note that the radiated power (panel (f)) was slowly increasing in the discharges with lithium conditioning; this is a commonly observed state when ELMs were avoided (panel (g)) with lithium evaporation in NSTX[10], thereby eliminating the associated periodic flushing of impurities. In addition the resulting profile changes changed neoclassical transport so that carbon and metallic impurities accumulated in the core, causing the temporal increase in radiated power.[23]

The SOLPS code[24] was used in interpretive analysis mode to quantify the changes in divertor recycling and cross-field transport. The procedure has been described elsewhere for the discharges with moderate boundary shapes[12, 13]. To summarize, the divertor D_α peak emission is the primary constraint on the divertor target recycling coefficient, the divertor peak heat flux is the primary constraint on the separatrix location in the reconstructed equilibrium (via power balance), and the density and temperature profiles are matched to determine the cross-field transport particle and thermal diffusivities. Because there are uncertainties with the ion profiles near the separatrix, SOLPS can be used to infer the change in electron transport in the edge region near the separatrix. Note that the simulations can only provide effective transport coefficients, i.e. separate diffusion and pinch terms are not accurately determined because this type of interpretive analysis is time independent.

Figure 6 shows the radial D_e and χ_e obtained from the SOLPS simulations to reproduce the measured profiles[22]. The D_e decreased monotonically inside the separatrix, by factors of 10-30x, when comparing the reference and highest lithium dose discharge. On the other hand, the χ_e increased by up to 10x in the last 1-1.5cm nearest the separatrix, but decreased by 5x

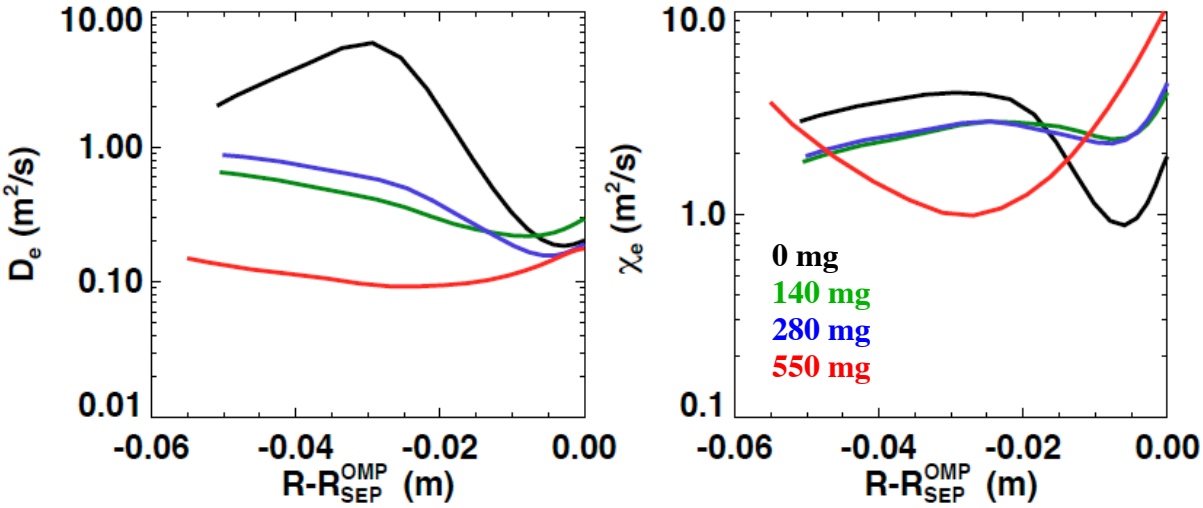

Figure 6: (a) effective electron particle diffusivity D_e and (b) electron thermal conductivity χ_e vs. distance from the separatrix at the outer midplane. The lithium evaporation dose is indicated.

inside of that region. The near-separatrix region increase in thermal transport can be understood conceptually because a higher diffusivity is needed to drive the same cross-field heat flux at the reduced edge density obtained with lithium conditioning, e.g. see the profile changes shown elsewhere[21]. The reduction in χ_e inside of that region was also observed with SOLPS analysis from the moderately shaped discharges; microstability analysis indicated a reduction in the drive for microtearing modes[25]. Additionally the divertor recycling coefficient dropped from 0.99-1.0 with no lithium to ~ 0.9 at the highest lithium dose[22]. In summary, the quantitative reduction in D_e and χ_e in these highly shaped discharges is very similar to those observed at moderate shaping[12, 20].

4. Summary and Implications for NSTX-U

In summary, we have reported on a systematic scan of the HeGDC time, applied before lithium evaporation, in NSTX, in an effort to determine the optimum operating procedure for NSTX-U. At constant external fueling and lithium evaporation, the discharge pulse length increased modestly with increasing HeGDC duration. Moreover the edge T_e and T_i increased moderately with increasing HeGDC duration at constant density and heating power. Furthermore, the divertor D_a emission in the far SOL increased when HeGDC was eliminated, but was otherwise unaffected by HeGDC duration. On the other hand, the near-SOL divertor D_a emission was unaffected by the duration of HeGDC. These results have practical implications for NSTX-U: a cycle of 3-5 min of HeGDC, followed by ~ 10 min of lithium evaporation is advocated, given the typical inter-discharge cycle time of 15-20 minutes. On the other hand, experiments that target maximizing performance should consider the use of longer HeGDC times, albeit at the cost of increasing the inter-discharge cycle time.

We have also used SOLPS modeling to quantify the reduction in divertor recycling and change in edge transport for low and high lithium dose, as compared to a reference boronized discharge without lithium, in a strongly shaped NSTX H-mode discharge. First the divertor recycling coefficient dropped from ~ 0.99 to 0.9. In addition, both the particle and electron thermal diffusivity dropped substantially in a broad region 1-4 cm radially inward of the separatrix, although electron transport within 1cm of the separatrix increased substantially. Overall the results parallel a comparable lithium dose scan conducted in moderately shaped discharges. These results also bode well for lithium usage to enhance plasma performance and reduce recycling in NSTX-U, which is designed to use a highly-shaped boundary plasma as in this study.

Acknowledgements

This research was sponsored in part by U.S. Dept. of Energy under contracts DE-AC02-09CH11466, DE-AC05-00OR22725, DE-FC02-04ER54698, DE-FC02-99ER54512 and DE-AC52-07NA27344. We gratefully acknowledge contributions of the NSTX operations staff.

References

1. C. H. Skinner *et al.*, *Nucl Fusion* **42** (2002) 329.

2. H. W. Kugel *et al.*, *J Nucl Mater* **313** (2003) 187.

3. R. Maingi *et al.*, *Phys Rev Lett* **88** (2002) 035003.

4. H. W. Kugel *et al*., *Phys Plasmas* **15** (2008) 056118.

5. H. W. Kugel *et al*., *J Nucl Mater* **363-365** (2007) 791.

6. H. W. Kugel *et al*., *J Nucl Mater* **390-391** (2009) 1000.

7. D. K. Mansfield *et al*., *Phys Plasmas* **3** (1996) 1892.

8. H. W. Kugel *et al*., *Phys Plasmas* **15** (2008) 056118.

9. M. G. Bell *et al*., *Plasma Phys Control Fusion* **51** (2009) 124054.

10. D. K. Mansfield *et al*., *J Nucl Mater* **390-391** (2009) 764.

11. R. Maingi *et al*., *Phys Rev Lett* **103** (2009) 075001.

12. J. M. Canik *et al*., *Phys Plasmas* **18** (2011) 056118.

13. J. M. Canik *et al*., *J Nucl Mater* **415** (2011) S409.

14. R. Maingi *et al*., *Nucl Mater Energy* (2016) submitted.

15. S. M. Kaye, and t. I. c. d. w. group, *Nucl Fusion* **37** (1997) 1303.

16. J. E. Menard *et al*., *Nucl Fusion* **52** (2012) 083015.

17. S. P. Gerhardt, R. Andre, and J. E. Menard, *Nucl Fusion* **52** (2012) 083020.

18. R. Maingi *et al*., *Phys Rev Lett* **107** (2011) 145004.

19. D. P. Boyle *et al*., *Plasma Phys Control Fusion* **53** (2011) 105011.

20. R. Maingi *et al*., *Nucl Fusion* **52** (2012) 083001.

21. R. Maingi *et al*., *J Nucl Mater* **463** (2015) 1134.

22. R. Maingi *et al*., *Fusion Eng Des* (2016) at press.

23. F. Scotti *et al*., *Nucl Fusion* **53** (2013) 083001.

24. R. Schneider, *Contrib Plasma Phys* **46** (2006) 3.

25. J. M. Canik *et al*., *Nucl Fusion* **53** (2013) 113016.